WEP Warwick Evans Publishing

International Journal of Natural Resources and Environmental Studies

ISSN: 3006-2012 (Print), ISSN: 3006-0834 (Online) | Volume 8, Number 4, Year 2026
DOI: https://doi.org/10.62051/ijnres.v8n4.11
Journal homepage: https://wepub.org/index.php/IJNRES/index

Numerical Study on the Particle Flow Behavior of Bolted Jointed Rock Mass under Impact-Shear Coupling

Qingshui Zhang*

School of Energy Science and Engineering, Henan Polytechnic University, Jiaozuo 454003, China
*Corresponding Author: Qingshui Zhang (Email: 15565347720@163.com)

ABSTRACT

To clarify the shear mechanical response and crack evolution of bolted jointed rock masses under impact disturbance, a mesoscopic particle flow model of the “rock mass-joint-bolt” system was established using PFC2D. The mechanical behavior and damage evolution of bolted jointed rock masses under impact-shear coupling were systematically investigated under different impact numbers, impact patterns, and confining pressures. The results show that, after impact disturbance, the shear stress-shear displacement curve of the bolted jointed rock mass can be divided into four stages: elastic stage, stress-drop stage, strengthening stage, and residual stage, while the normal displacement-shear displacement curve undergoes three stages: shear contraction, dilation, and softening. With the increase in impact parameters, the shear modulus, peak shear stress, and residual strength generally decrease, the normal restraint capacity weakens, the joint closure increases, and the peak normal displacement decreases. With increasing confining pressure, the shear strength and residual bearing capacity are enhanced, whereas the dilation behavior is significantly restrained. Based on the evolution law of normal displacement, the peak dilation angle was defined and its degradation characteristics were analyzed. The results indicate that the peak dilation angle generally shows a trend of initial increase followed by decrease with increasing impact parameters, while its attenuation coefficient increases with confining pressure. Crack evolution analysis further shows that impact disturbance significantly promotes internal crack propagation in bolted jointed rock masses, and the number of cracks increases with impact parameters. As confining pressure increases, the total number of cracks further increases, whereas the proportion of tensile cracks decreases slightly. The study can provide a reference for the stability analysis and support design of bolted jointed rock masses subjected to impact disturbance.

KEYWORDS

Bolted Jointed Rock Mass; Impact Disturbance; Shear Behavior; Dilation Angle; Crack Evolution; Particle Flow Numerical Simulation.

1. INTRODUCTION

The study of the static and dynamic responses of anchored jointed rock masses is an important interdisciplinary field in rock mechanics and engineering applications. In recent years, researchers have systematically investigated a series of key scientific issues, including the anchorage mechanism of rock bolts, interface shear characteristics, dynamic impact-induced damage, and the stability of anchorage systems, through experimental studies, numerical simulations, and theoretical analyses. These studies have revealed the influence of bolt inclination, anchorage length, confining pressure, and dynamic disturbance on anchorage performance, and have established various mechanical models and optimized support schemes, thereby providing an important theoretical basis and engineering guidance for the anchorage design of deep rock masses.

Chang et al.[1]investigated the stress wave propagation law and spalling failure characteristics of prestressed end-anchored bodies under different impact air pressures based on SHPB tests, established a spalling damage model for the anchored body, and verified it using a high-speed camera. Li Haibin et al.[2]established a mechanical analysis model based on beam theory for the condition where the shear direction is perpendicular to the bolt inclination. By comprehensively considering the factors affecting the shear resistance of the bolt, they derived and verified a calculation formula for the bolt shear resistance. Liu Quansheng et al.[3]established a theoretical calculation model for the shear strength of bolted joints, verified the model, and discussed the effects of bolt inclination, surrounding rock compressive strength, bolt diameter, and normal stress on the shear strength of bolted joints. Liu Xuesheng et al.[4]obtained the movement characteristics of the lateral roof at different stages in deep gob-side roadways through similar simulation experiments, established a structural mechanical model, proposed a quantitative calculation method, revealed the energy-driven mechanism of failure instability, and put forward instability risk classification and control technology. Qiu Pengqi et al.[5]used a split Hopkinson pressure bar to study the impact failure response of four types of anchored rock specimens under impact dynamic loading, analyzed the influence of anchorage mode on the dynamic crack initiation and propagation of bolted rock specimens, and proposed the concept of impact resistance timeliness of anchored rock. Song Yang et al.[6]took red sandstone, limestone, and basalt as research objects, established a mechanical model for bolted jointed rock masses by combining experimental results, statically determinate beam theory, and the principle of minimum residual energy, and proposed the optimal anchorage angle based on theoretical formulas. Tang Xudong et al.[7]found through interface shear tests that mortar strength directly affects the peak strength and shear stiffness of the interface; under the same mortar strength, the peak strength, shear stiffness, and residual shear strength of the interface are proportional to the normal stress; when the normal stress is fixed, an increase in shear rate leads to an increase in peak shear strength, but has little effect on residual shear strength. Wu Yongzheng et al.[8–9]comparatively analyzed the changes in the mechanical properties of bolts before and after impact loading through field and laboratory tests, as well as the effects of impact energy and bolt mechanical properties on the mechanical behavior of rock masses. Zhan Sai et al.[10], focusing on the influence of anchorage defects, carried out uniaxial compression tests and, combined with acoustic emission, distributed optical fiber, and DIC techniques, identified precursory fracture characteristics and clarified the influence of defect location on bearing performance and failure mode. Zhao Zenghui et al.[11–12], considering the coupling effect among the rock block, bonding layer, and bolt in anchored rock masses, established a three-dimensional model of bolted jointed rock masses, verified its reliability, and further analyzed the effects of anchorage angle and joint morphology on the overall shear resistance and progressive damage behavior of each component.

Chen et al.[13]investigated the reinforcement and crack-arresting mechanisms of bolted fractured granite through dynamic impact tests and numerical simulations. The results showed that anchorage can significantly improve the compressive resistance of rock masses, reduce energy absorption, increase energy transmission, and effectively suppress the propagation of intergranular cracks. Fan et al.[14]used SHPB tests to study the dynamic response and energy dissipation characteristics of fractured and anchored rock masses, and found that rock bolts can significantly enhance the support capacity of fractured rock masses against dynamic disturbance, and that this enhancement increases as the anchorage angle decreases. Li et al.[15]established a damage constitutive model for anchored jointed rock masses under coupled static and fatigue loading, and found that fatigue loading weakens the specimen strength and increases deformation, while static loading has a cumulative degradation effect. Song et al.[16], combining the GTN model and Weibull distribution, established a shear damage constitutive model for prestressed anchored jointed rock masses and verified its accuracy through experiments and simulations. Wang et al.[17]compared the damage evolution and acoustic emission characteristics of intact rock and rock reinforced with constant-resistance energy-absorbing bolts through rockburst tests, and found that high-strength energy-absorbing bolts can effectively reduce the risk of rockburst. Wu et al.[18], based on direct shear tests on rough joints, studied the

shear responses of fully grouted bolts and energy-absorbing bolts, and found that the ultimate shear displacement of energy-absorbing bolts is greater than that of fully grouted bolts. Zhu et al.[19], through a large number of tests on blocky rock masses with and without bolting, found that the number of bolts has a significant effect on the peak strain and uniaxial compressive strength of the rock mass, and established an analytical prediction model based on the Winkler beam model, which was verified by the above experiments. Zheng et al.[20]compared the mechanical responses of energy-absorbing bolts and fully grouted bolts in jointed rock masses through laboratory shear tests, and found that the former has stronger adaptability and energy absorption capacity under high-speed shear, whereas the latter exhibits higher peak shear stress.

In summary, although considerable progress has been made in the study of impact disturbance effects and the mechanical response of anchored jointed rock masses, systematic research under complex conditions such as multi-field coupling and the superposition of dynamic and static loads is still insufficient, and a complete theoretical framework has not yet been established. In particular, the nonlinear influence of dynamic impact parameters, such as impact number and impact pattern, on the degradation of shear stiffness and dilation angle of bolted jointed rock masses remains unclear. Therefore, this study adopts a numerical simulation method to systematically analyze the shear mechanical properties of jointed rock masses after bolting under different impact disturbance parameters and confining pressure conditions, and further reveal the mechanical failure mechanism of anchored jointed rock masses under impact-shear action.

2. PARTICLE FLOW SHEAR SIMULATION OF BOLTED JOINTED ROCK MASS

In the study of jointed rock masses subjected to impact disturbance and shear action, the macroscopic mechanical response can only reveal the overall variation pattern of the system, but it is difficult to reflect the specific mechanism of the bolt during damage propagation and energy transfer. Therefore, in this study, a mesoscopic particle flow model based on the interaction among the “rock mass-joint-bolt” was established to investigate the mechanical response and damage evolution characteristics of the bolted structure under coupled impact-shear loading from the microscopic perspective.

2.1. Calibration of Mesoscopic Model Parameters

To obtain representative mesoscopic parameters for the numerical model, the particle parameters of each component were adjusted and optimized repeatedly using the trial-and-error method. By analyzing the mechanical response of the model under different parameter combinations, a set of parameters that could better characterize the shear and deformation characteristics of the jointed rock mass was selected. The optimized results are shown in Table 1.

Table 1 Mesoscopic parameters of the bolted jointed specimen

	Parameter	Value
Rock particles	Minimum radius / mm	0.45
	Maximum radius / mm	0.6
	Porosity	0.07
	Friction coefficient	0.5
	Elastic modulus / GPa	3.95
	Stiffness ratio	1.5
	Effective modulus of parallel bond / GPa	3.96
	Stiffness ratio of parallel bond	1.45
	Cohesion of parallel bond / MPa	12
	Tensile strength of parallel bond / MPa	5.0
	Friction angle of parallel bond / °	0.1

2.2. odel Establishment

The numerical model was established with dimensions of 200 mm in length and 100 mm in width, and PFC2D was adopted to carry out numerical simulation of the shear test on anchored infilled joints. The model consists of the upper rock mass, lower rock mass, bolt, anchoring agent, and joint structural plane. The joint structural plane was realized by importing the joint profile curve. In the model, blue particles represent the rock mass, red particles represent the anchoring agent, green particles represent the bolt, and the curve represents the joint structural plane. For the rock particles, the parallel bond model was adopted, while the particle contacts in the vicinity of the joint profile curve were defined using the smooth joint model.

In this study, a shear box system was constructed using rigid boundary elements, and the whole structure was divided into upper and lower parts. The upper shear box consists of wall elements W2, W5, and W6, and a fixed boundary condition was applied through horizontal displacement constraints (); the lower shear box consists of wall elements W1, W3, and W4, which remained in a stationary constrained state during the impact loading stage (), and then switched to displacement loading mode during the shear stage. A staged loading strategy was adopted in the system. During the impact stage, both the upper and lower shear boxes were maintained under fixed constraints to ensure the stability of energy transfer. After the impact energy was fully dissipated, the lower shear box was subjected to one-way shear loading along the horizontal direction at a preset rate, while the upper shear box remained under displacement constraint throughout the entire process.

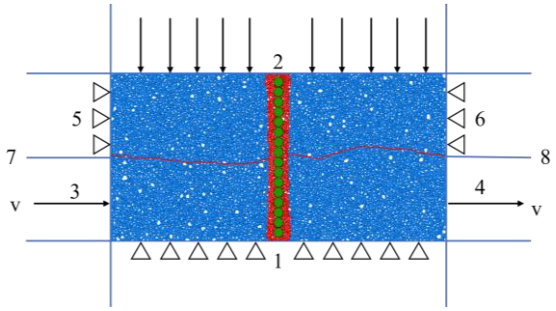

Figure 1 Schematic diagram of the numerical model of bolted jointed rock mass

2.3. Realization of Impact Loading

Referring to the pendulum impact principle used in impact tests, an impact block was arranged on the upper right side of the jointed rock mass model, and an appropriate distance was reserved between its initial position and the rock mass to avoid geometric interference. To create an open impact space and ensure the authenticity and effectiveness of the loading process, unnecessary constraint boundaries during the collision process were removed, and only the upper wall (W2) was retained as the loading boundary, so that the impact block could strike the rock mass freely. The dynamic behavior of the impact block was controlled through loop statements by assigning its initial velocity, impact times, and loading pattern, and an automatic reset condition was set. After each impact, the block automatically returned to its initial coordinate position to ensure the same initial state for each impact, thereby eliminating the interference of residual displacement and stress. After the completion of the impact stage, the previously removed walls were reloaded and the impact block was deleted so as to restore the structural integrity of the model.

The application process of impact loading is shown in Figure 2. To further analyze the influence of different impact disturbance intensities and confining pressure conditions on the mechanical response of the jointed rock mass, multiple numerical simulation schemes were designed, and the corresponding parameters are listed in Table 2.

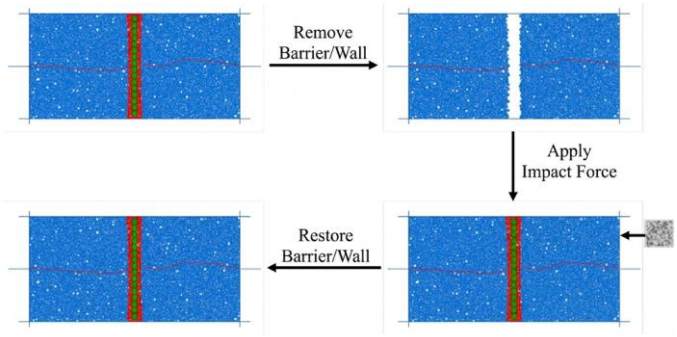

Figure 2 Flowchart of impact loading application

Table 2 Test schemes

Scheme No.	Impact times	Impact pattern	Confining pressure/MPa
AI	0, 1, 2, 3, 4, 5	Constant	2
AII	1, 2, 3, 4, 5	Increasing	2
AIII	5	Constant	0, 4, 6
AIV	5	Increasing	0, 4, 6

3. NUMERICAL SIMULATION RESULTS AND ANALYSIS OF MECHANICAL BEHAVIOR

3.1. Shear Stress–Shear Displacement Curves

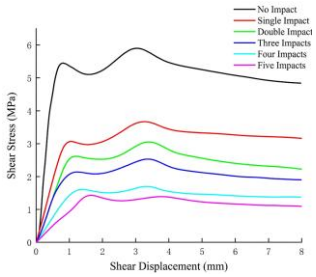

a. Shear stress–displacement curves of bolted jointed rock mass after constant impact damage under 2 MPa

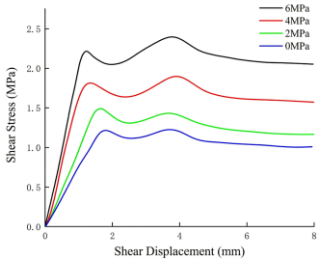

b. Shear stress curves under different confining pressures after five constant impacts

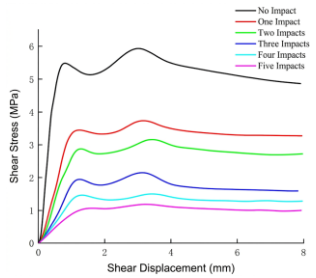

c. Shear stress–displacement curves of bolted jointed rock mass after increasing impact damage under 2 MPa

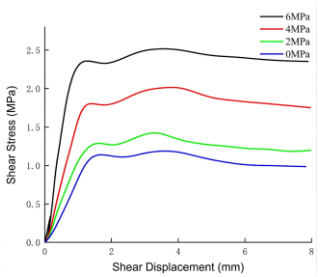

d. Shear stress curves under different confining pressures after five increasing impacts

Figure 3 Shear stress–shear displacement curves of jointed rock mass after damage under different conditions

Figures 3(a)–3(d) show the shear stress–shear displacement curves of bolted jointed rock mass specimens after impact disturbance. Overall, the stress–displacement curves of the bolted specimens

clearly exhibit a complete evolution process from linear elastic deformation to residual strength, showing four stages: “elastic response–local failure–strength recovery–stable friction”.

At the initial stage of shearing, the specimen shows an obvious linear growth trend, indicating that a relatively strong interlocking effect still exists between the joint surfaces. The shear strength at this stage reflects the ability of the joint surface to resist shear deformation. However, after impact disturbance, it decreases significantly. Under constant impact conditions, when the number of impacts increases from 0 to 5, the shear modulus, which depends on the slope of the stress–displacement curve in the elastic stage, gradually decreases from 7.91 GPa/m to 0.93 GPa/m. Under increasing impact conditions, the shear modulus decreases from 7.31 GPa/m to 0.80 GPa/m. This indicates that impact loading weakens the mechanical coupling capacity between the joint surfaces. Meanwhile, an increase in confining pressure can offset this weakening effect to a certain extent. For example, under five constant impacts, when the confining pressure increases from 0 MPa to 6 MPa, the shear modulus increases from 0.71 GPa/m to 1.98 GPa/m. Under increasing impact conditions, it correspondingly increases from 0.79 GPa/m to 2.50 GPa/m. This indicates that higher confining pressure helps restrain crack propagation and improves the deformation resistance of the system.

As the shearing process continues, the stress curve shows an obvious decline, indicating that local asperities on the joint surface are worn or sheared off, and the rock mass enters the plastic damage stage, while the anchorage system is still in a load-bearing state. Subsequently, the curve rises again, showing a significant strengthening trend, indicating that the bolt activates the secondary load-bearing potential of the rock mass through the combined action of interface friction and axial restraint. Under different impact intensities, the peak shear stress gradually decreases with increasing disturbance degree. Under constant impact conditions from 0 to 5 impacts, the peak shear stress decreases from 5.90 MPa to 1.43 MPa. Under increasing impact conditions, it decreases from 5.93 MPa to 1.18 MPa. Confining pressure also has a significant influence on peak strength. Under five constant impacts, as the confining pressure increases from 0 MPa to 6 MPa, the peak shear stress increases from 1.23 MPa to 2.40 MPa. Under increasing impact conditions, it increases from 1.18 MPa to 2.51 MPa, indicating that confining pressure has a clear strengthening effect on the shear strength of the joint surface.

In the later stage of shearing, the curve gradually becomes flat and the system enters the residual stage. At this stage, both the bolt and the surrounding rock are damaged, and the overall load-bearing capacity stabilizes at a relatively low level. Under constant impact conditions, the residual strength decreases from 4.84 MPa to 1.09 MPa. Under increasing impact conditions, it decreases from 4.86 MPa to 1.00 MPa. An increase in confining pressure can also effectively improve the residual bearing capacity. Under five constant impacts, the residual strength increases from 1.01 MPa to 2.05 MPa, while under increasing impact conditions it increases from 0.98 MPa to 2.35 MPa. Overall, impact disturbance weakens the shear resistance of bolted jointed rock mass, whereas the increase in confining pressure compensates for the strength loss to some extent, making the system exhibit a more stable mechanical response.

3.2. Normal Displacement–Shear Displacement Curves

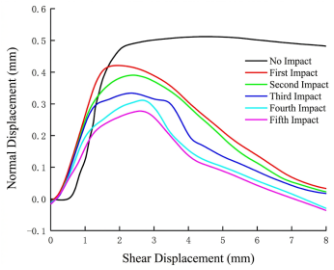

a. Normal displacement–shear displacement curves under different constant impacts at 2 MPa

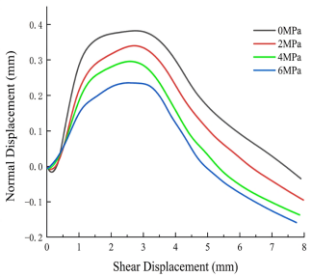

b. Normal displacement–shear displacement curves under different CNS conditions with constant impact

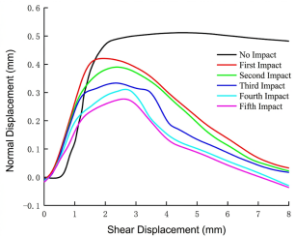

c. Normal displacement–shear displacement curves under different increasing impacts at 2 MPa

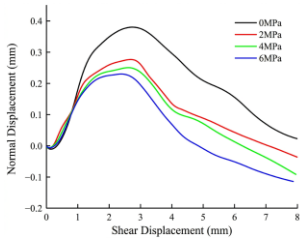

d. Normal displacement–shear displacement curves under different CNS conditions with increasing impact

Figure 4 Normal displacement–shear displacement curves of bolted jointed rock mass after damage under different conditions

Figures 4(a)–4(d) show the relationship curves between normal displacement and shear displacement of damaged bolted jointed rock mass under different conditions. Overall, the bolted jointed rock mass exhibits obvious shear contraction and shear dilation during the shearing process, and its evolution can be divided into three stages: shear contraction, shear dilation, and softening. This reflects the nonlinear deformation behavior of the anchorage system under impact disturbance.

In the shear contraction stage, the normal displacement shows a downward trend, indicating that the joint surface closes during the initial shearing process. As the number of impacts increases, the restraining capacity of the bolt gradually weakens, and the amount of shear contraction continues to increase. Under constant impact conditions, the shear contraction increases from −0.003 mm at 0 impacts to −0.010 mm at 5 impacts. Under increasing impact conditions, it increases from −0.003 mm to −0.013 mm. Confining pressure significantly restrains deformation at this stage. Higher confining pressure enhances the overall constraint on the rock mass and significantly reduces the joint closure. When the confining pressure is 0 MPa, 2 MPa, 4 MPa, and 6 MPa, respectively, the shear contraction of the specimen under five constant impacts is −0.015 mm, −0.009 mm, −0.006 mm, and −0.002 mm, respectively. Under increasing impact conditions, the values are −0.011 mm, −0.009 mm, −0.006 mm, and −0.004 mm, respectively.

After entering the shear dilation stage, the normal displacement changes from decreasing to increasing, and the shear slip of local asperities on the joint surface causes volume expansion of the rock mass. However, with the accumulation of impact disturbance, the roughness of the joint surface decreases, and both the peak normal displacement and its growth rate decrease to varying degrees. Under constant impact conditions from 0 to 5 impacts, the peak normal displacement decreases from 0.51 mm to 0.34 mm. Under increasing impact conditions from 1 to 5 impacts, it decreases from 0.42 mm to 0.28 mm. An increase in confining pressure further restricts the climbing behavior of the joint surface, significantly slowing down the dilation rate. When the confining pressure increases from 0 MPa to 6 MPa, the peak normal displacement under five constant impacts decreases from 0.38 mm to 0.24 mm, while under increasing impact conditions it decreases from 0.37 mm to 0.23 mm. This

indicates that under high confining pressure conditions, the deformation of the joint surface is restricted and the dilation effect is significantly suppressed.

In the softening stage, the normal displacement decreases again. The deformation behavior at this stage is mainly affected by damage to the anchorage module and wear of the joint surface. Impact disturbance weakens the restraining effect of the bolt, and increased wear makes the joint surface smoother. The increase in normal force induced by shear slip causes the joint closure effect to dominate again, and the rock mass structure gradually enters a stable residual state.

Overall, impact disturbance weakens the normal restraint capacity of the bolted jointed rock mass, resulting in an increase in shear contraction and a decrease in shear dilation amplitude. However, an increase in confining pressure offsets this weakening effect to a certain extent and enhances the normal stability of the joint surface.

During the shear deformation process of bolted jointed rock mass, the evolution of the dilation angle is influenced not only by the geometric morphology and mechanical characteristics of the joint surface, but also by the complex coupling with the mechanical response of the bolt reinforcement system. The relative slip of the joint surface induced by shear loading, together with bolt restraint, causes the normal displacement and shear displacement to exhibit obvious stage characteristics. Since the dilation angle defined in this paper is intended to characterize the overall macroscopic dilation effect of the rock mass, the displacement process when the asperities enter the plastic deformation stage is regarded as the key node at which macroscopic structural stress drop occurs. Accordingly, the dilation angle corresponding to this stage is defined as the peak dilation angle, which reflects the volume deformation characteristics and the evolution law of joint surface morphology of the bolted jointed rock mass near the peak strength.

3.3. Damage Analysis of Bolted Jointed Rock Mass during Shearing

Based on the evolution law of normal displacement during the shearing process of bolted jointed rock mass, this study analyzes joint surface damage and dilation behavior. The local non-uniform dilation behavior of the joint surface is treated as an integral whole, and an overall dilation angle representing the macroscopic volume change characteristics of the rock mass is defined to reflect the macroscopic dilation effect of the jointed rock mass during shearing. This mechanical process can be decomposed into two competing mechanisms: the joint closure effect and the asperity climbing effect.

At the initial stage of shearing, the joint closure effect dominates, and the rock mass exhibits shear contraction characteristics. The mechanical response at this stage is mainly controlled by three factors. First, the asperities are in the elastic stage, and their deformation is constrained by the constitutive properties of the material. Second, the initial normal stress determines the degree of contact tightness of the joint surface. Third, the presence of confining pressure restrains the rapid development of normal displacement. At this time, the joint asperities can be regarded as contact units undergoing purely elastic deformation.

With the continuous increase of shear displacement, the asperities gradually enter the climbing stage. When the normal upward displacement caused by climbing exceeds the closure amount, the normal displacement of the rock mass begins to increase and the system enters the shear dilation stage. When the shear stress exceeds the elastic limit of the asperities, local plastic deformation and wear begin to occur, corresponding to the post-peak stage of the shear stress curve. At this time, the destruction of asperities causes the macroscopic dilation effect of the joint surface to gradually weaken, and the overall dilation angle correspondingly degrades.

As pointed out by Ban Liren [21], the evolution law of the dilation angle can directly reflect the wear evolution state of joint surface asperities. Combined with the above analysis, it can be seen that the normal displacement of the jointed rock mass is composed of the closure displacement of joint asperities and the upward displacement caused by the climbing effect.

The normal displacement caused by the climbing effect can be expressed as:

$$\Delta v_1 = \Delta s_p \tan\psi \tag{2.1}$$

where Δv_1 is the climbing displacement, Δs_p is the plastic shear displacement, and ψ is the dilation angle.

At the same time, considering the closure deformation of the joint under normal stress, the rough joint surface is equivalent to a continuously distributed asperity group. Since the climbing and closure behaviors of asperities with different inclination angles are different, it can be assumed that the joint closure displacement is positively correlated with the shear displacement and the dilation angle, namely:

$$\Delta v_2 = \beta \Delta s_p \tan\psi \tag{2.2}$$

where Δv_2 is the joint closure displacement, β is the shear closure coefficient, and Δs_p is the shear displacement.

Considering both mechanisms comprehensively, the total normal displacement of the jointed rock mass can be expressed as:

$$\Delta v = \Delta v_1 - \Delta v_2 \tag{2.3}$$

Where Δv is the normal displacement.

According to the relationship between the normal displacement and shear displacement curves, the instantaneous dilation angle of the jointed rock mass after the asperities begin to wear can be obtained as:

$$\psi = \arctan\left(\frac{\Delta v}{\Delta s_p (1-\beta)}\right) \tag{2.4}$$

Since this paper assumes that the asperities of the jointed rock mass do not wear during the elastic stage, but begin to wear after the peak of the shear stress curve, the dilation angle of the jointed rock mass at the moment corresponding to the peak shear stress is defined as the peak dilation angle. This angle also represents the maximum macroscopic dilation effect of the rock mass under the peak load-bearing state.

By fitting the normal displacement–shear displacement curves obtained from the simulation, the joint closure coefficient is determined to be 0.6. This coefficient mainly depends on the material properties of the rock mass and is independent of changes in boundary conditions[21]. Substituting this parameter into the above equations yields the dilation angle degradation curve (see Figure 5). The results show that, as the shearing process proceeds, the joint asperities are gradually worn, and the dilation angle gradually decreases and eventually approaches zero. This law is consistent with the findings of Barton [22].

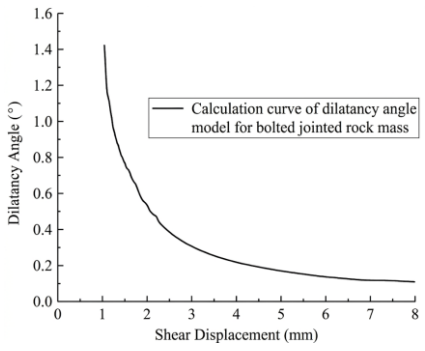

Figure 5 Calculated curve of dilation angle for undamaged jointed rock mass

3.3.1. Effect of Impact Disturbance on Peak Dilation Angle

Based on the dilation angle calculation model established above, the evolution law of the peak dilation angle of jointed rock mass under different impact parameters is obtained by calculation, and the specific data are shown in Table 3.

It can be found that under the initial impact, the bolt reinforcement module is damaged, the restraining effect of the bolt weakens, and the peak dilation angle of the specimen increases. One constant impact causes the peak dilation angle to increase by 14.31%, while one increasing impact causes it to increase by 11.93%. However, as the number of impacts increases, joint surface wear intensifies. At the same time, the restraint of the bolt aggravates local stress concentration, which further causes joint surface wear, and the peak dilation angle begins to decrease again, showing a trend of increase followed by decline. Under constant impact conditions from 2 to 5 impacts, the increases in peak dilation angle are 12.04%, 8.43%, 5.15%, and 3.23%, respectively. Under increasing impact conditions from 2 to 5 impacts, the increases are 10.28%, 9.24%, 4.33%, and 3.47%, respectively.

Table 3 Peak dilation angle parameters of bolted jointed rock mass under different impact disturbances

Impact times	Peak dilation angle / °			
	Constant impact	increase	Increasing impact	increase
0	1.42273	—	1.42773	—
1	1.62632	14.31%	1.64172	11.93%
2	1.67893	12.04%	1.60732	10.28%
3	1.59571	8.43%	1.50380	9.24%
4	1.51074	5.15%	1.43353	4.33%
5	1.44013	3.23%	1.59246	3.47%

3.3.2. Constraining Effect of Confining Pressure on Shear Damage

Table 4 shows the variation of the peak dilation angle of bolted jointed rock mass under different confining pressure conditions. It can be found that, as the confining pressure gradually increases, the peak dilation angle of the jointed rock mass shows a continuous downward trend under both constant cyclic impact and increasing cyclic impact conditions. This phenomenon indicates that higher confining pressure significantly restrains the deformation of the joint surface, weakens the climbing and extension effects of joint asperities, and thus reduces the overall dilation capacity of the rock mass.

Table 4 Peak dilation angle parameters of bolted jointed rock mass under different confining pressures

Confining pressure / MPa	Peak dilation angle / °			
	Five constant impacts	Decrease	Five increasing impacts	Decrease
0	1.43664	—	1.428380	—
2	1.50272	4.60%	1.489371	4.27%
4	1.39561	1.83%	1.386573	1.40%
6	1.45099	2.88%	1.449932	2.95%

This result is consistent with the findings of Wu Jiahong [23]. As the confining pressure increases, the normal displacement of the joint surface rises, leading to an enhancement of the normal stress borne by the joint surface, so that the “climbing” deformation of the asperities during shearing is significantly suppressed, thereby causing a reduction in the peak dilation angle. In addition, under the same impact energy conditions, different impact patterns have different effects on the peak dilation angle of the jointed rock mass, and the peak dilation angle is lower under increasing impact conditions. The main reason lies in the cumulative damage effect of increasing impact: the gradually increasing

impact energy causes joint asperities to continuously exceed the strength threshold, inducing more extensive fatigue damage. The microcracks formed by previous impacts provide propagation paths for subsequent impacts, accelerating the damage evolution of the joint surface and the degradation of the dilation angle. In contrast, constant impact exhibits a certain degree of local adaptability. Under continuous fixed-energy impact, the rock mass forms a local damage saturation zone, and the subsequent impact energy is mainly dissipated through existing cracks, so its overall degradation rate is relatively slower. In order to quantify the dynamic degradation behavior of the dilation angle during shearing, this study introduces an attenuation coefficient, whose physical meaning is the relative attenuation rate of the dilation angle per unit shear displacement. Based on the exponential fitting of the test data (Figure 6), the evolution equation of the dilation angle can be expressed as:

$$\theta = \theta_0 \cdot e^{-\eta\delta} \tag{2.5}$$

where θ is the dilation angle, θ_0 is the peak dilation angle, η is the attenuation coefficient, and δ is the shear displacement.

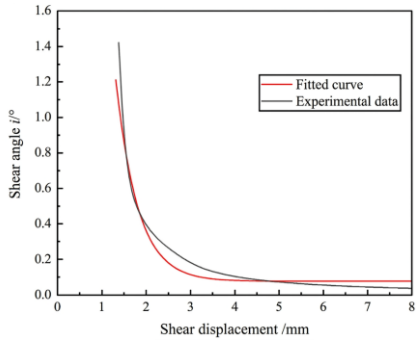

Figure 6 Fitting curve of dilation angle degradation

The calculation results show that the attenuation coefficient of the dilation angle of bolted jointed rock mass differs significantly under different confining pressure conditions (see Table 5). As the confining pressure increases, the attenuation coefficient shows an overall upward trend. When the confining pressure increases from 0 MPa to 6 MPa, the attenuation coefficient under constant impact conditions increases by 84.60%, while under increasing impact conditions it increases by 55.15%. This result indicates that a high confining pressure environment significantly suppresses the dilation behavior of the jointed rock mass. Under higher normal stress constraint, joint asperities are more likely to undergo wear and crushing during shearing, leading to a faster degradation rate of the dilation angle and thus a further increase in the attenuation coefficient.

Table 5 Attenuation coefficient values of bolted jointed rock mass under different confining pressures

Confining pressure / MPa	Attenuation coefficient η			
	Five constant impacts	Increase	Five increasing impacts	Increase
0	1.1226	—	1.3397	—
2	1.3347	18.89%	1.6111	20.26%
4	1.5768	40.46%	1.9644	46.63%
6	2.0723	84.60%	2.0785	55.15%

4. EVOLUTION AND DISTRIBUTION CHARACTERISTICS OF CRACKS

4.1. Crack Evolution Characteristics of Bolted Jointed Rock Mass under Impact Loading

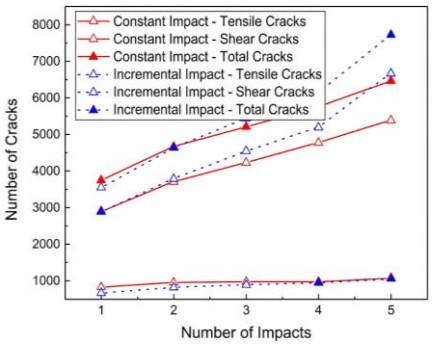

Figure 7 Number of cracks in bolted jointed rock mass under different impact parameters

Figure 7 shows the variation in crack number of the bolted jointed rock mass under different impact patterns. Under constant impact conditions, the number of cracks in the jointed rock mass increased progressively from the initial 1743 to 2169, 2425, 2684, and 2902, with growth rates of 24.44%, 11.80%, 10.68%, and 8.12%, respectively. It can be seen that, in the early stage of constant impact loading, crack propagation was relatively rapid, and then gradually slowed down. The increase in the total number of cracks decreased overall, showing a certain saturation trend. In terms of crack type, tensile cracks always dominated, and their proportion increased with the number of impacts, rising successively from 76.75% to 79.87%, 81.33%, 83.01%, and 83.12%.

Under the increasing impact pattern, the number of cracks in the jointed rock mass increased progressively from 1550 to 2023, 2377, 2653, and 3132, with growth rates of 30.51%, 17.50%, 11.61%, and 18.05%, respectively. Different from the constant impact case, the crack number under increasing impact still maintained significant growth in the later stage, indicating that high-amplitude impact energy induced stronger cumulative damage at later stages and made crack propagation more intense. In terms of crack type distribution, the proportion of tensile cracks under increasing impact was significantly higher than that under constant impact and also showed a continuous upward trend, reaching 75.77%, 78.98%, 82.10%, 83.45%, and 85.72%, respectively. This indicates that high-amplitude increasing impact not only accelerated the crack evolution process inside the jointed rock mass, but also strengthened the dominant role of tensile failure in the overall damage mode.

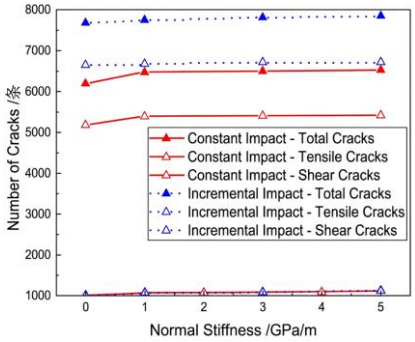

Figure 8 Number of cracks in bolted jointed rock mass under different confining pressure conditions

Figure 8 shows the influence of different confining pressure levels on the crack number of the bolted jointed rock mass under the same impact parameters. The results indicate that, with increasing confining pressure, the total number of cracks in the bolted jointed rock mass exhibited a slight upward trend. Under constant impact conditions, the crack number increased progressively from 2877 to 2902, 3011, and 3214. Although the crack number increased slightly, tensile cracks still dominated, and their proportions were 83.68%, 83.12%, 82.13%, and 81.02%, respectively, showing a slight decreasing trend.

Under increasing impact conditions, the crack number increased progressively from 2984 to 3132, 3126, and 3317, and the overall trend was similar to that under constant impact conditions. Tensile

cracks were still the main crack type, and their overall proportion was higher than that under constant impact conditions, being 86.70%, 85.72%, 84.84%, and 83.95%, respectively, also showing a slight downward trend.

This phenomenon can be attributed to the fact that, under high confining pressure, that is, a high-stiffness boundary, the overall deformation of the rock mass is significantly constrained and the shear sliding capacity is reduced. However, under the restraining effect of the bolt, stress concentration is more likely to occur in local regions, causing the impact energy to preferentially act in the interaction zone between the joint surface and the bolt, thereby promoting crack initiation and propagation and leading to a slight increase in crack number with increasing confining pressure. Overall, under high confining pressure, the fracture pattern of the bolted jointed rock mass becomes more complex, showing a competition between local concentrated failure and overall confinement effects.

4.2. Crack Evolution and Distribution Characteristics under Impact Loading and Shear Action

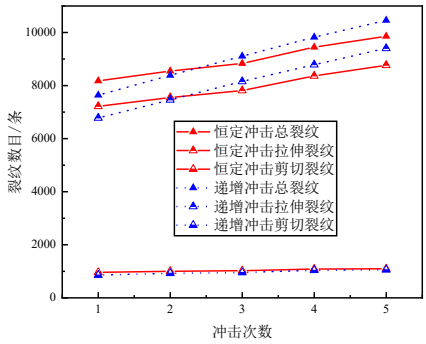

Figure 9 Number of cracks in bolted jointed rock mass after shearing under different impact disturbances

During the shearing process, by statistically analyzing the crack evolution characteristics of the bolted jointed rock mass under different impact disturbance patterns and confining pressure conditions, the variation laws of the crack number and tensile crack proportion after shearing can be obtained, as shown in Figures 9 and 10. Under constant impact disturbance, the number of cracks after the end of shearing increased with impact number, reaching 3876, 3994, 4129, 4356, and 4499, respectively, while the proportions of tensile cracks were 85.47%, 86.21%, 87.15%, 88.04%, and 88.91%, respectively. It can be seen that, with the increase in the number of impact disturbances, the crack number showed a clear upward trend, and the proportion of tensile cracks increased synchronously. Under increasing impact disturbance, the numbers of cracks after shearing were 3721, 3927, 4237, 4483, and 4773, respectively, while the proportions of tensile cracks were 85.67%, 86.33%, 87.45%, 88.54%, and 89.01%, respectively. In general, both the crack number and the tensile crack proportion increased with the number of impacts. Under the same impact energy conditions, increasing impact disturbance caused more cracks and a higher proportion of tensile cracks than constant impact disturbance, indicating that the cumulative energy effect made crack propagation within the jointed rock mass more significant.

Under different confining pressure conditions, the crack distribution after shearing also showed similar. When subjected to five constant impact disturbances, the crack numbers under confining pressures of 0, 2, 4, and 6 MPa were 4387, 4499, 4678, and 4815, respectively, and the corresponding proportions of tensile cracks were 89.77%, 88.91%, 88.03%, and 87.67%. When subjected to five increasing impact disturbances, the crack numbers were 4621, 4773, 4834, and 4912, respectively, and the corresponding proportions of tensile cracks were 89.91%, 89.01%, 88.72%, and 88.11%. The results show that, with increasing confining pressure, that is, stiffness, the total number of cracks gradually increased, whereas the proportion of tensile cracks showed a decreasing trend. This is because, under high-stiffness conditions, the overall deformation of the jointed rock mass is restricted,

making it difficult for energy to be released through deformation. Meanwhile, the presence of the bolt provides a channel for energy transfer, causing crack propagation to become more concentrated and more dominated by shear cracks, thereby resulting in an increase in total crack number but a decrease in the proportion of tensile cracks.

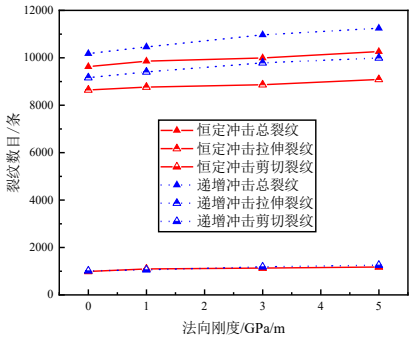

Figure 10 Number of shear cracks in bolted jointed rock mass after disturbance under the same impact parameters and stiffness conditions

5. CONCLUSIONS

This study systematically analyzed the mechanical response and crack evolution characteristics of bolted jointed rock masses during shear processes under impact and post-impact disturbance by means of numerical simulation. From a mesoscopic perspective, the influence of impact parameters and confining pressure on the mechanical properties of anchored jointed rock masses was revealed. The main conclusions are as follows:

(1) The shear stress curve of the bolted jointed rock mass after impact disturbance can be divided into four stages: the elastic stage, stress-drop stage, strengthening stage, and residual stage. With the increase in impact parameters, the shear modulus, peak stress, and residual strength all show a decreasing trend, whereas an increase in confining pressure leads to corresponding increases in these parameters. The normal displacement curve experiences three stages: shear contraction, dilation, and softening. With the application of impact disturbance, the restraining effect of the bolt weakens, the closure displacement of the joint surface increases, and the peak normal displacement decreases. However, with increasing confining pressure, both exhibit a decreasing trend.

(2) The dilation angle corresponding to the turning point of stress reduction was defined as the peak dilation angle. The results show that the peak dilation angle increases with increasing impact parameters, and exhibits an “increase–decrease” characteristic under high impact parameters. Meanwhile, the attenuation coefficient of the peak dilation angle increases with increasing confining pressure, indicating that the dilation behavior of the jointed rock mass is restrained under high confining pressure conditions.

(3) During the shear process under impact and post-impact disturbance, the number of internal cracks in the jointed rock mass increases significantly with the increase in impact parameters, whereas the number of cracks during the post-disturbance shear process is slightly lower than that under pure shear conditions. With increasing confining pressure, both the total number of cracks and the peak inter-particle contact force show an increasing trend, indicating that stress concentration inside the rock mass becomes more significant under high confining pressure, and that crack propagation and energy transfer are more pronounced.

REFERENCES

[1] Chang Jucai, Qi Chao, Yin Zhiqiang, et al. Study on the mechanical response characteristics of end-anchored anchorage bodies under dynamic loading [J]. Rock and Soil Mechanics, 2022, 43(12): 3294-3304.

[2] Li Haibin, Tan Hanhua, Yuan Wei, et al. Study on the anchorage mechanism of bolts under the condition that the shear direction is perpendicular to the bolt inclination [J]. Chinese Journal of Applied Mechanics, 2021, 38(05): 1995-2003.

[3] Liu Quansheng, Lei Guangfeng, Peng Xingxin, et al. Study and experimental verification of the shear mechanical model of bolts in jointed rock mass [J]. Chinese Journal of Geotechnical Engineering, 2018, 40(05): 794-801.

[4] Liu Xuesheng, Wang Xin, Tan Yunliang, et al. Energy-driven mechanism of failure and instability of anchored surrounding rock in deep gob-side roadways [J]. Journal of China Coal Society, 2024, 49(04): 1819-1833.

[5] Qiu Pengqi, Ning Jianguo, Wang Jun, et al. Experimental study on the impact-resistance timeliness of bolted rock mass under impact dynamic loading [J]. Journal of China Coal Society, 2021, 46(11): 3433-3444.

[6] Song Yang, Fan Bo, Wang Heping. Study on the shear mechanical model of bolted jointed rock mass considering normal stress and rock strength [J]. Chinese Journal of Rock Mechanics and Engineering, 2023, 42(06): 1325-1335.

[7] ang Xudong, Zhang Jiachi, Nie Wen. Experimental study on the mechanical properties of fully grouted bolt anchorage units [J]. Mechanics in Engineering, 2023, 45(05): 1044-1056.

[8] Wu Yongzheng, Fu Yukai, Hao Dengyun. Study on the dynamic response law of bolted rock mass under lateral impact loading [J]. Chinese Journal of Rock Mechanics and Engineering, 2020, 39(10): 2014-2024.

[9] Wu Yongzheng, Chen Jinyu, Jiao Jiankang, et al. Damage and failure mechanism of anchored surrounding rock under impact loading [J]. Journal of China Coal Society, 2018, 43(09): 2389-2397.

[10] Zhan Sai, Guan Kai, Zhu Wancheng, et al. Study on the uniaxial compression fracture mechanism of jointed specimens with anchorage defects based on acoustic emission [J]. Journal of Mining and Strata Control Engineering, 2024, 6(04): 80-90.

[11] Zhao Zenghui, Sun Wei, Liu Hao, et al. Analysis of the dynamic shear response of anchorage systems in jointed rock mass under impact loading [J]. Journal of Mining and Strata Control Engineering, 2022, 4(05): 72-80.

[12] Zhao Zenghui, Liu Hao, Sun Wei, et al. Progressive failure behavior of rock mass anchorage systems considering interface and damage effects [J]. Rock and Soil Mechanics, 2022, 43(11): 3163-3173.

[13] Chen Y , Yu D , Wang Y , et al. Dynamic Characteristics and Anchorage Mechanisms of Fractured Granite: Analytical, Numerical and Experimental Analyses[J]. Rock Mechanics and Rock Engineering, 2024, 58(2): 1-21.

[14] Fan D , Liu X , Tan Y , et al. Energy mechanism of bolt supporting effect to fissured rock under static and dynamic loads in deep coal mines[J]. International Journal of Mining Science and Technology, 2024, 34(3): 371-384.

[15] Li Y , Huang D , He J . Energy evolution and damage constitutive model of anchored jointed rock masses under static and fatigue loads[J]. International Journal of Fatigue, 2023, 167(PA): 107313.

[16] Song Y , Li Y . Study on the constitutive model of the whole process of macroscale and mesoscale shear damage of prestressed anchored jointed rock[J]. Bulletin of Engineering Geology and the Environment, 2021, 80(8): 1-14.

[17] Wang Q , Wu W , Wang Y , et al. Evolution and Control Mechanism of Rockburst in Rock Anchored by New Energy-Absorbing Material[J]. Rock Mechanics and Rock Engineering, 2023, 56(6): 4569-4582.

[18] Wu X , Zheng H , Jiang Y . Influence of joint roughness on the shear properties of energy-absorbing bolt[J]. International Journal of Rock Mechanics and Mining Sciences, 2023, 163: 105322.

[19] Zhu C , Xing X , He M , et al. Failure behavior and strength model of blocky rock mass with and without rockbolts[J]. International Journal of Mining Science and Technology, 2024, 34(6): 747-762.

[20] Zheng H , Wu X , Jiang Y , et al. Insights into velocity-dependent shear characteristics of bolted rock joints: A comparative study of fully-grouted and energy-absorbing bolts[J]. International Journal of Rock Mechanics and Mining Sciences, 2024, 183: 105910-105910.

[21] Ban Liren, Du Weisheng, Hou Yuhang, et al. Prediction model for the dilation law of soft rock joints considering the degradation of actual contact three-dimensional roughness [J]. Chinese Journal of Geotechnical Engineering, 2024, 46(05): 1008-1017.

[22] Barton N Review of a new shear-strength criterion for rock joints[J]. Engineering Geology, 1973, 7(4): 287-332.

[23] Wu Jiahong, Liu Jie, Song Yanbin. Numerical simulation of rock joint dilation characteristics under constant normal stiffness boundary conditions [J]. Journal of Mining and Strata Control Engineering, 2022, 4(02): 71-81.

[24] Wu Jiahong, Liu Jie, Song Yanbin. Numerical simulation of the shear dilation characteristics of rock joints under constant normal stiffness boundary conditions [J]. Journal of Mining and Strata Control Engineering, 2022, 4(02):71-81.